A Lagrangian numerical investigation of the origins and fates of the salinity maximum water in the Atlantic

Bruno Blanke and Michel Arhan
Laboratoire de Physique des Océans, CNRS-IFREMER-UBO, Brest, France

Alban Lazar
Laboratoire d'Océanographie Dynamique et de Climatologie, CNRS-IRD-UPMC, Paris, France

Gwenaëlle Prévost
Laboratoire de Physique des Océans, CNRS-IFREMER-UBO, Brest, France

Received 21 January 2002; revised 26 April 2002; accepted 15 May 2002; published 18 October 2002.

[1] The origins and fates of the Atlantic salinity maximum water (SMW), formed through excess evaporation in the tropics and subtropics of both hemispheres, are studied using monthly mean outputs of a numerical simulation of the world ocean climatological circulation. After defining formation domains from the surface salinity field and the vertical stratification, a Lagrangian technique is used to estimate the formation rates and main pathways in each hemisphere and the role of this water in the framework of the warm water return flow of the meridional overturning cell. Formation rates around 9 and 11 Sv are found in the Southern and Northern Hemispheres, respectively. While the export of the southern SMW from its formation area is realized by the western boundary currents, that of the northern SMW mainly results from interior subduction. Equatorward of the formation regions, a fraction of each SMW variety is entrained in the subtropical cells that connect the subtropics to the equatorial region. Poleward of them, both varieties are seen to feed the regions of subtropical mode water (STMW) formation around 35° of latitude in both hemispheres. The bulk of the transport associated with each variety eventually turns northward: This amounts to ~6 Sv of southern SMW gathered in the North Brazil Undercurrent (NBUC), and ~10 Sv of northern SMW found in the Gulf Stream at 35°N, of which 8 Sv have gone through the Caribbean Sea. Of the 13.4-Sv northward transport of the meridional overturning cell estimated by the model at 47°N, more than 50% (6.9 Sv) is found to have transited through at least one of the SMW regions. This gives an indication of the likely important role of SMW formation in the observed northward salinity increase of the upper Atlantic Ocean. *INDEX TERMS:* 4283 Oceanography: General: Water masses; 9325 Information Related to Geographic Region: Atlantic Ocean; 4255 Oceanography: General: Numerical modeling; 4532 Oceanography: Physical: General circulation

Citation: Blanke, B., M. Arhan, A. Lazar, and G. Prévost, A Lagrangian numerical investigation of the origins and fates of the salinity maximum water in the Atlantic, *J. Geophys. Res.*, *107*(C10), 3163, doi:10.1029/2002JC001318, 2002.

1. Introduction

[2] The high salinities of the North Atlantic upper layers, through their preconditioning effect on the formation of North Atlantic Deep Water, are a key element of the global thermohaline circulation [*Broecker*, 1991; *Gordon*, 1996]. At the southern boundary of the Atlantic Ocean, the relatively low latitude of the southern tip of Africa (35°S) is often thought to contribute to this salinity signal by making way to an import of salty Indian Ocean water and, conversely, to a partial export of fresher water from the South Atlantic Current [*Reid*, 1961; *Gordon et al.*, 1992]. The net evaporative character of the Atlantic [*Baumgartner and Reichel*, 1975] is naturally another factor to which the high salinities of the upper ocean can be related [*Gordon and Piola*, 1983; *Broecker*, 1991]. This second mechanism acts through the formation of surface salty water in the tropics and subtropics of both hemispheres, under the effect of net positive evaporation minus precipitation fluxes, and subsequent lateral redistribution of this water by the upper circulation.

[3] The high salinity surface water is sometimes named Subtropical Underwater (STUW) [e.g., *O'Connor et al.*, 1998], on account of its subduction beneath fresher waters, or salinity maximum water (SMW) [*Worthington*, 1976; *Stramma and Schott*, 1996]. Here we use the latter terminology, which conveys better the idea of the water signature. The SMW is formed by vertical homogenization of the surface layer (with convection maintained by dominant evaporation processes), before subduction within the per-

0148-0227/02/2002JC001318$09.00

manent thermocline. Using hydrographic sections, *Tsuchiya et al.* [1992, 1994] evidenced the SMW signature in the subtropics of both hemispheres and diagnosed its spreading from subsurface salty extensions. The SMW in the North Atlantic was discussed by *Worthington* [1976], who described its formation in the upper 200 m of the approximate latitude range 20°N–30°N, with a salinity maximum extending southwestward below fresher equatorial water. In the same hemisphere, *Hernandez-Guerra and Joyce* [2000] observed SMW entering the Caribbean Sea and *Schmitz and Richardson* [1991] noted its presence in the Straits of Florida. *Sprintall and Tomczak* [1992] pointed out its role in the establishment of the "barrier layer" which limits downward the surface mixed layer in the northwest equatorial Atlantic. *Taft* [1963] associated the salty waters of the Equatorial Undercurrent (EUC) with a southern subtropical origin, and *Wacongne and Piton* [1991] used this SMW signal to trace the EUC to the approaches of Africa. At 38°S and 42°S in the western Argentine Basin, *Gordon* [1981] observed cores of high salinity water of subtropical origin near 100 m-depth in the Brazil Current (BC) extension and recirculation, and pointed out the effects of this water on the characteristics of the subtropical mode water (STMW) formed in this region.

[4] To our knowledge, the only study dedicated to the SMW is that of *O'Connor et al.* [1998] in the Pacific Ocean. In the Atlantic, partial information can be gained from the occasional observations quoted above and from recent works on the subtropical cells (STCs) that connect the subtropical and equatorial domains [*Malanotte-Rizzoli et al.*, 2000]. There has been no thorough investigation of the SMW in this ocean, of its meridional spreading away from the formation areas, and of the contrasted behaviors in both hemispheres. In this study we propose a description of the SMW based on the Lagrangian analysis of a numerical simulation. Lagrangian diagnostics applied to the output of climatological ocean general circulation models (OGCMs) indeed prove useful in determining global or basin scale circulation schemes. We analyze the monthly archive of a simulation run with the *Océan Parallélisé* (OPA) model, forced by climatological atmospheric fluxes and constrained on observational climatologies for temperature and salinity. These constraints ensure the reproduction of a stable seasonal cycle propitious to offline Lagrangian computations. Section 1 briefly presents the numerical tools (OGCM simulation and Lagrangian interpretation) and a comparison of SMW zonal transports calculated from the model and available observations. Section 2 introduces the definition we adopted for the SMW formation rate, in terms of physical mechanism and geographical positioning in both hemispheres. In section 3 we discuss the immediate fate of these waters by means of Lagrangian diagnostics. Remote destinations (obtained with extended trajectory computations) are presented in section 4. The origins of the waters that participate in SMW formation are studied in section 5, before a conclusion is drawn in section 6.

2. Numerical Tools and Model-Data Comparison

2.1. The Ocean Model

[5] We use the OPA model [*Madec et al.*, 1998] in its global configuration. The domain extends from the Southern Ocean at 78°S to 90°N. The singularity of the North Pole is removed by introducing an appropriate coordinate transformation that includes a double, numerical inland pole. As a result, the zonal resolution is 2° within the whole Southern Hemisphere (hereafter SH) and slightly distorted north of 20°N. The meridional grid interval varies from 0.5° at the equator, to a maximum of 1.9° in the subtropics. There are 31 levels in the vertical, with the highest resolution (10 m) in the upper 150 m. The bottom topography and coastlines are derived from *Smith and Sandwell*'s [1997] study complemented by values from the $5' \times 5'$ ETOPO5 data set at the northernmost latitudes. A daily climatology obtained from the ECMWF 15-yr (1979–1993) reanalyses and smoothed by an 11-day running mean was used to force the model at the surface. The experiment was designed to recover and study the dynamics associated with the observed global ocean hydrography. Therefore, our analyses are carried out over the last 12 months of a 10-year simulation in which a restoring term to the *Levitus* [1982] climatology was added to the potential temperature and salinity equations [*Madec and Imbard*, 1996]. This Newtonian damping acts everywhere except in the 20°S–20°N latitude band and in the surface mixed layer (in order not to interfere with the model's fast adjustment in these regions). Its intensity is defined as the inverse of a timescale that varies from 50 days in the upper ocean to 360 days at 5000 m, to account for slower dynamic adjustments at depth. The constraint is also slightly relaxed poleward of 50°N and 50°S where observations are sparser. The damping comes progressively to zero within 1000 km from the coastlines as boundary currents may not be well captured by the climatology. The model physics (isopycnal lateral mixing, 1.5 order vertical turbulent closure scheme) is able to recover the boundary and equatorial currents not well resolved in the *Levitus* [1982] climatology.

2.2. Lagrangian Interpretation

[6] The equations of the OGCM are discretized on a C-grid. This description is ideal for the computation of analytical mass-preserving streamlines of a sampled velocity field [*Blanke and Raynaud*, 1997]. Assuming that velocity is constant over periods equal to the sampling time of the OGCM output, one may associate successive segments of such streamlines to actual three-dimensional (3D) trajectories of fictive fluid particles. The notion of a mass-preserving Lagrangian scheme is essential for water mass tracing, since it ensures that the calculated trajectories mimic the genuine movement of the water parcels, without intercepting the coastline or ocean bottom. As proposed by *Döös* [1995] and adapted by *Blanke and Raynaud* [1997], the description of a water mass may be achieved by inseminating it on a given geographic section with hundreds of thousands of particles, each of which being associated with an infinitesimal transport. Infinitesimal volumes of water are conserved along the model streamlines and, for selected final destinations, the infinitesimal transports may be added and directional transports produced. Off-line diagnostics allow backward computations of trajectories and the joint use of backward and forward calculations provides an estimation of the methodological error made in computing transports. Moreover, off-line diagnostics permit to loop over a climatological year while calculating trajec-

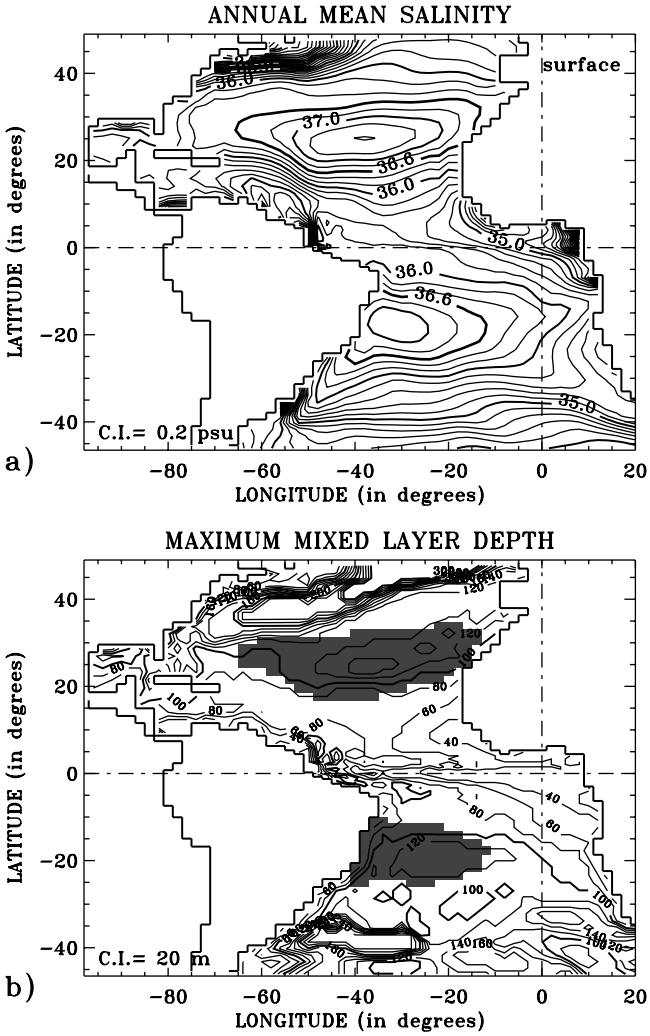

Figure 1. (a) Annual mean surface salinity with a 0.2 psu contour interval. (b) Annual maximum depth of the surface mixed layer, with shading of the region of annual mean surface salinity larger than 36.6 psu.

tories, without the constraint of the true length of the OGCM simulation for setting up the limits of the Lagrangian integration. Finally, circulation schemes may be obtained by computing the horizontal stream function related to the vertical integration of the 3D transport field determined by the particle displacements of a water mass [*Blanke et al.*, 1999].

2.3. First Validation of Model Results

[7] As the fresh water flux imposed at the sea surface includes a relaxation term to the *Levitus* [1982] salinity climatology, there is only little difference between model surface salinity monthly maps and the climatology. Subtropical latitudes are characterized by salinity maximums, slightly higher on an annual mean in the Northern Hemisphere (NH, 37.4 psu) than in the SH (37.0 psu) (Figure 1). The two areas of high surface salinity are centered at comparable longitudes (30°W–35°W), and at latitudes (25°N, 18°S) that are symmetric with respect to that of the Intertropical Convergence Zone (ITCZ). The northern feature is somewhat wider than the southern one (see the 36.6 isohaline). While the latter is observed adjacent to the coast of America, fresher waters of equatorial origin separate the former from the continent.

[8] Comparisons of meridional salinity sections from the model (Figure 2) with direct measurements from individual hydrographic lines (not shown) assessed the model fair ability to account for the large scale vertical distributions in both areas. In the NH, the individual transect used for the comparison was a section at 35°W carried out in August 1983 (cruise 104 of R/V *Knorr*) [*McCartney*, 1993]. In the SH, we used section A17 of the World Ocean Circulation Experiment realized in February 1994 at the nominal longitude of 30°W [*Mémery et al.*, 2000]. The mean depth and slopes of the isohalines are well depicted by the model, although the equatorial pycnocline is not pinched enough.

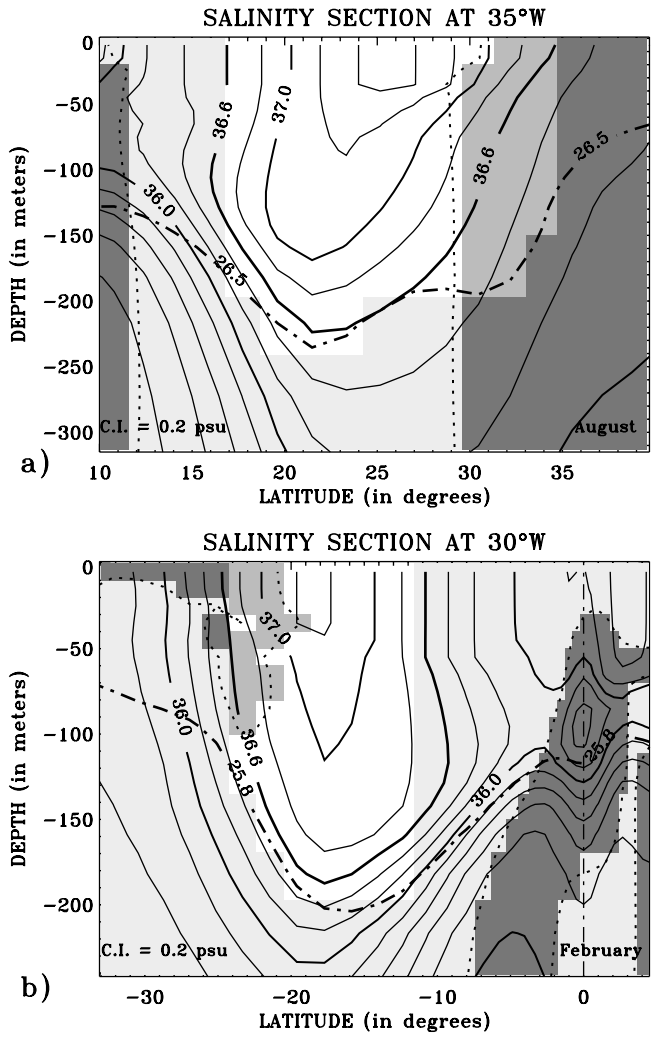

Figure 2. Monthly mean meridional salinity sections from the model. (a) At 35°W in August; (b) at 30°W in February. The dashed-dotted line shows the isopycnal used as the lower bound of each salinity patch for the transport computations in section 2.3. Light gray shading refers to the outside of the salinity patch, medium gray bounded by dotted lines to areas where the zonal velocity is eastward, and dark gray to regions where both criteria are met. The SMW transports discussed in section 2.3 are calculated in the white domain.

Table 1. Comparison of Westward Salty Water Exports (Sv) Diagnosed From the Model and From Observations[a]

Hemisphere	Observations	Model
Northern	2.4	2.7
Southern	12.5 (9.0)	7.2

[a] For the Northern (*Knorr* cruise 104, 35°W) and Southern (A17, 30°W) Hemispheres.

The salinity maximum associated with the EUC is visible (Figure 2b). The model outcrop positions of the isohalines are generally satisfactory, except at the northern boundary of the southern SMW, where the value S = 36.6 psu is found at 11°S in the model section (Figure 2b) and at 8°S in A17 [*Wienders et al.*, 2000, Figure 8a]. The combination of sharp surface salinity meridional gradients in the observations and a strong lateral smoothing in the Levitus field (which is used as a relaxation term in the model) probably explains the difference.

[9] We compared the volume transports within each salinity patch in the model and the measured sections (Table 1). Computations of the latter used geostrophy referenced at 2000 dbar. Both patches were bounded meridionally at the outcropping of the 36.6 isohaline. Vertically, they were limited by an isopycnal with a mean depth calibrated on the same salinity contour, namely 26.5 kg/m^3 (respectively 25.8 kg/m^3) for the NH (SH). The westward geostrophic transports calculated from the data showed little sensitivity (±0.5 Sv, 1 Sv $\equiv 10^6$ m^3 s^{-1}) to variations of the reference level between 1500 and 2500 dbar. Estimates of the westward Ekman transports derived from the wind stress used to force the model amount to 1.9 Sv (respectively 0.1 Sv) for the northern (southern) patch. This component strengthens the differences shown in Table 1 between the geostrophic and model-based volume transports. This difference is weak in the NH but quite significant south of the equator. As noted above, the region where the surface salinity exceeds 36.6 in the southern SMW is narrower in the model (25°S to 11°S) than in the A17 section (25° to 8°S). Limiting the geostrophic calculation to the exact band of latitude covered by the model leads to a weaker transport estimate (9.0 Sv, bracketed in Table 1) closer to the model estimate and probably compatible with it given the uncertainty of the geostrophic computation. This high sensitivity of the model transports to the exact location of the northern border of the southern SMW results from the South Equatorial Current (SEC) being intense in this region [*Wienders et al.*, 2000]. As the formation rates presented below are essentially different from horizontal transports and are representative of yearlong processes over the SMW area, there is no reason why they should be subject to the same sensitivity. The underestimation of the southern SMW area hinted by this one-dimensional comparison, if real throughout the year, could nevertheless be associated with some underestimation of the formation rates as well.

3. SMW Formation Rate

3.1. Standard Approaches

[10] Several methods are usually followed to compute water mass transformation rates in a given density range. The dynamic method [*Stommel*, 1979; *Marshall et al.*, 1993] directly diagnoses the volume flux into the main thermocline by computing the subduction rate across the winter mixed-layer base. It requires the evaluation of the wind-driven Ekman flux, part of which results in a diapycnal mass transfer. The thermodynamic method [*Walin,* 1982] lies on volume and buoyancy budgets. Water mass transformation rates are inferred from air-sea heat and fresh water fluxes, under the assumption of negligible lateral contributions. *Speer and Tziperman* [1992] and *Speer et al.* [1995] used such calculations for deriving water mass transformations in the Atlantic Ocean from the COADS data set. As emphasized by *Marshall et al.* [1999], both approaches are formally equivalent in the context of coast-to-coast integrations and in the absence of diffusive processes acting on the volume of fluid under consideration. A third method was proposed by *Jenkins* [1987, 1988] and employed to estimate mixing parameters or integral subduction and ventilation rates from the age of a given tracer field. *O'Connor et al.* [1998] used it to derive the formation rate of the SMW in the Pacific from chlorofluorocarbon data, and made a successful comparison with estimates based on the dynamic method. A fourth method, based on Lagrangian calculations, was proposed first by *Woods* [1985] and applied to OGCMs by *Williams et al.* [1995] and *Qiu and Huang* [1995]: annual mean subduction rates may be calculated from the tracing of particles released at the base of the winter mixed layer.

3.2. Our Methodology

[11] Like the fourth method mentioned above, our approach is based on the Lagrangian analysis of numerical OGCM simulations. However, it incorporates more accuracy in the initial positioning of selected particles and fully uses the information recorded along individual trajectories. It was previously applied to the study of the global ocean [*Blanke et al.*, 2002a] for which ventilation diagnostics were derived regardless of the water mass properties. A zoom of the results obtained by *Blanke et al.* [2002a] over the Atlantic is given in Figure 3. The equatorial and eastern coastal rails reveal upwelling of subsurface water into the

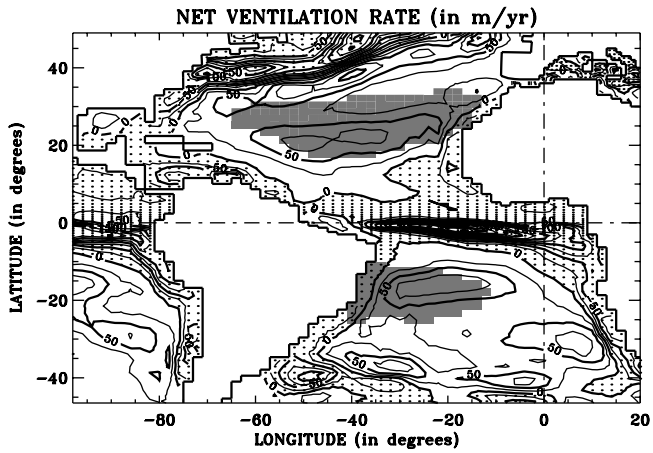

Figure 3. Net ventilation rate for the Atlantic Ocean contoured with a 25 m/yr contour interval, as diagnosed by *Blanke et al.* [2002a]. Dotted areas refer to movements from the interior ocean to the surface mixed layer (obduction). The SMW formation regions are shaded.

mixed layer. The tropical and subtropical bands (40°S–10°S, and 10°N–40°N) exhibit an obvious inclination for subduction, as in the Eulerian calculation of *Lazar et al.* [2002]. In the STMW formation region at northern mid-latitudes (35°N–45°N), the ventilation pattern matches previous observation-based estimates [*Marshall et al.*, 1993]. However, the corresponding positive (respectively negative) values of up to 100 m/yr (−200 m/yr) are smaller than those obtained by *Williams et al.* [1995] from the CME (Community Model Experiment) simulation of the Atlantic basin. This discrepancy is probably due to stronger mixed layer variations or lateral circulation at these latitudes in the CME simulation.

3.3. SMW Formation Areas

[12] As this study is dedicated to a specific water mass, we need a definition of the SMW formation areas in both hemispheres. As introduced in section 2 and illustrated in Figure 1b, two criteria are applied. The first one refers to the saline character of the water and limits the formation areas laterally at the 36.6 surface isohaline. The second one recognizes its pycnostad character and limits it vertically to the base of the surface mixed layer, using a 0.01 kg/m3 threshold in density. These criteria are consistent with the mechanism of SMW formation, namely a surface salinization under a positive evaporation minus precipitation fresh water flux, followed by a vertical homogenization within the surface mixed layer, before a lateral or vertical export (by subduction) out of the formation domain.

[13] The envelope of each salinity patch moves with time, and the model offers only a discrete representation (with successive monthly mean states) for it. Therefore, as introduced by *Blanke et al.* [2002a], the volume flux escaping this region is described in two complementary ways. We first document the advective transfer to the interior ocean or to neighboring regions with particles during each month of the climatological year. Next we describe the flux expulsed from the salinity patch on the occasion of abrupt (monthly) modifications of its structure (such as mixed layer shallowing, or lateral retraction of the salinity patch). The total number of particles we use is over several million as any of them explains only a fraction of the total transport, not to exceed a prescribed maximum value per documented month (in this case 10^{-3} Sv) [*Blanke and Raynaud*, 1997; *Blanke et al.*, 1999]. These particles will be intercepted over convenient geographical sections (introduced in the next paragraph) to investigate the fates of SMW, eliminating those returning to their initial salinity patch, as such particles do not correspond to genuine SMW export. In this way, the Lagrangian analysis can differentiate detrainment into the seasonal pycnocline from true ventilation (injection of mass within the permanent pycnocline) as the first process corresponds to short journeys of the particles, without export from the initial SMW area.

[14] The 3D trajectories of the particles initially located over the envelope of each salinity patch are integrated till they reach one of the sections shown in Figure 4. In the NH, a section located at 69°W intercepts the flow that enters the Caribbean Sea and a section at 35°N intercepts the SMW that flows northward without transiting through the Caribbean. A transatlantic section at 10°N intercepts the particles with equatorward trajectories. As the Straits of Florida are a one way passage in the model, no westward interception is required there. An equivalent approach is used for the southern salinity patch: the same 10°N section is used to quantify the northward export of southern SMW. A section at 30°S intercepts the southward flowing SMW. A section located at 15°W across the equator quantifies the fraction of SMW participating in an equatorial eastward redistribution of mass (mostly within the EUC). This section is connected to Africa with a zonal segment at 6°S. As already specified, all the particles that recirculate within their initial salinity patch are filtered out from further calculation as they do not refer to true SMW export.

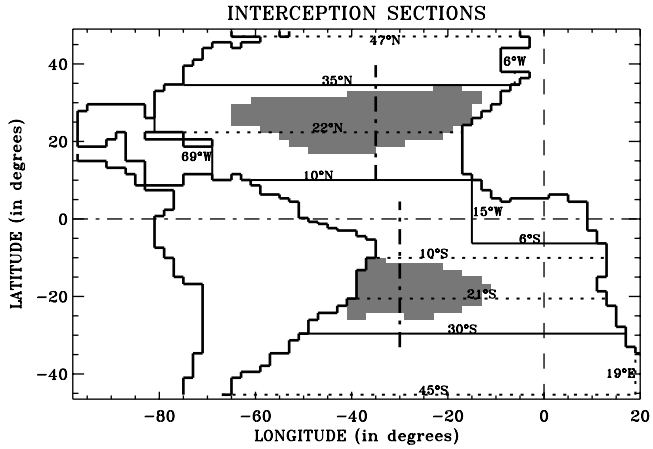

Figure 4. Interception sections used for the Lagrangian analysis. Thick lines refer to the initial study of SMW export (sections 3 and 4). Dotted lines refer to extended Lagrangian calculations (section 5). The tracks of the hydrographic sections (35°W and 30°W) drawn in Figure 2 are also shown (dashed-dotted). SMW formation regions are shaded.

3.4. SMW Formation Rates

[15] Summing the infinitesimal transports associated with the particles explaining SMW export from the formation areas provides estimates of its formation rate. We find 11.3 Sv (respectively 8.6 Sv) for the NH (SH). All Lagrangian computations discussed in this paper were run backward and forward (see section 2.2), with resulting transport differences smaller than 0.1 Sv (as a measure of the accuracy of the method). Sensitivity studies (Table 2) showed that these estimates depend poorly on the density criterion used to define the vertical extent of the formation domains, but that they are more sensitive to its lateral definition based on a surface isohaline, as a weaker salinity leads to larger formation regions and, therefore, to higher formation rates. In Figure 1b, the contour S = 36.6 psu is seen to encompass regions of higher mixed layer depth indicative of Mode Water formation in both hemispheres, but the main reason that led us to choose this particular isohaline lies in the North Atlantic. With this definition, the northern boundary of the SMW in this basin is close to 30°N (Figure 1) and nearly coincident to the line of convergence of the Ekman transports of the westerlies and trade winds (not shown), which is a natural barrier to the meridional spreading of surface waters. Although there is no such coincidence in the SH (the poleward side of the S > 36.6 psu domain is about 5

Table 2. SMW Formation Rates (Sv) Computed for Both Hemispheres[a]

	36.6 psu, 10^{-2} kg/m^3	36.6 psu, 5×10^{-3} kg/m^3	36.6 psu, 2×10^{-2} kg/m^3	36.4 psu, 10^{-2} kg/m^3	36.8 psu, 10^{-2} kg/m^3
NH	11.3	10.9	11.6	N/A	8.3
SH	8.6	8.4	8.7	11.2	6.2

[a]The first column expresses results obtained for standard criteria on surface salinity and vertical density threshold. Following columns report sensitivity tests on these criteria. No result could be obtained with a 36.4 psu salinity in the Northern Hemisphere as the corresponding salinity patch extends beyond the interception sections.

degrees to the north of the Ekman transport convergence), and a slightly lower surface salinity limit (36.4 psu) could have been used there, we preferred to use the same value in both basins. Finally, and as mentioned above, we have confirmation that the SMW formation rates do not match the westward transports of Table 1: zonal movements within a formation area as calculated in section 2 do not necessarily lead to true SMW export, and, moreover, a significant fraction of the subduction is in fact achieved by means of a vertical export. Finally, the results prove little sensitive to the location of the interception lines, provided that the latter do not intercept the formation areas and encompass decently the domain in study.

3.5. Mechanism of SMW Subduction

[16] In Figure 3, two regions of high ventilation rates near 15°S and 20°N (>50 m/yr) correspond to the subduction of the SMW. For a better understanding of these subduction maxima we used the kinematic formulation of the Eulerian annual subduction rate proposed by *Nurser and Marshall* [1991]:

$$S_{\mathrm{ann}} = -(U_{\mathrm{H}} \cdot \mathbf{grad}\, H + W_{\mathrm{H}}) \qquad (1)$$

where S_{ann} is the annual volume flux across z = − H(x, y) representing the base of the deepest mixed layer throughout the year (Figure 1b), and U_H and W_H are the annual mean horizontal and vertical velocity at depth H. This approximate representation of permanent subduction has the advantage of a clear legibility of the main processes at play, namely lateral subduction induced by horizontal currents across sloping parts of the mixed layer bottom, and vertical subduction.

[17] A quantification of both processes was made. The vertical contribution was found close to the Ekman pumping field. Considering lateral subduction, we mentioned above the near coincidence of the SMW formation areas with regions of deeper mixed layer in both hemispheres (Figure 1b), a consequence of this water being a mode water formed by convection driven by air-sea fluxes. The two regions are crossed by the North Equatorial Current (NEC) and the SEC, which both have a westward and equatorward orientation. Therefore, when transported equatorward by these currents out of the formation domains, the SMW finds itself in regions of shallower surface mixed layer, which causes a lateral subduction of its deeper part. As a result, the contribution of lateral subduction was found highest on the equatorward sides of the formation regions where the lateral gradient of the mixed layer depth is most pronounced. Overall, the lateral and vertical contributions were found of equal importance in both SMW regions, and the total formation rate found using the formulation of *Nurser and Marshall* [1991] was comparable to the Lagrangian calculation.

4. SMW Export From the Formation Regions

4.1. Northern SMW

[18] Figure 5 depicts the transfers of northern SMW to any of the three relevant interception sections. In a manner

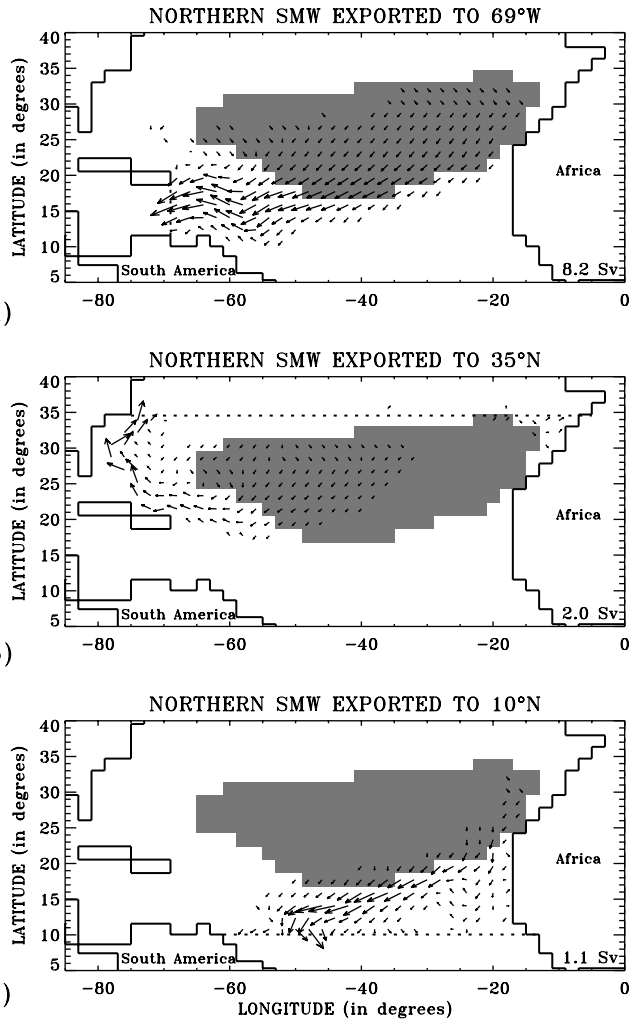

Figure 5. Vertically integrated transport of the northern SMW transported to remote interception sections. Arrows' size is normalized by the length of the largest transport of each panel, and smaller transports are enlarged for better readability. (a) Transmission to the Caribbean Sea (69°W). (b) Direct transmission to 35°N. (c) Transmission to 10°N. The region of formation of northern SMW is shaded on each panel.

similar to that of *Blanke et al.* [1999], the graph is obtained by summing algebraically the infinitesimal transports associated with the particles. This sum is calculated on the velocity grid points of the staggered C-grid [*Arakawa* 1972], at each junction of two model grid cells. Northward, eastward, and upward movements are counted positive, while southward, westward and downward movements are counted negative. The resulting 3D transport field corresponds to the SMW flow from its formation area to the final interception section considered. Integrating this field vertically gives a two-dimensional (2D) transport field that we display by means of vectors, or, whenever no particle initialization or interception occurs within the horizontal domain, by means of a horizontal stream function [*Blanke et al.*, 1999].

[19] Most of the flow enters the Caribbean Sea (Figure 5a, 8.2 Sv, 73%). Only 2 Sv (18%) of the newly formed SMW directly reaches 35°N, avoiding the Caribbean Sea (Figure 5b). A small fraction of it (0.3 Sv) is directed toward the Gulf of Cadiz, and eventually feeds the Mediterranean inflow at Gibraltar. As the SMW that transits through the Caribbean Sea eventually flows northward through the Straits of Florida (see below), the amount of northern SMW found to contribute directly to the salinity increase of the North Atlantic denser waters is 10.2 Sv. The remaining 1.1 Sv (10%) reach 10°N (Figure 5c). Two ensembles of particles are found at 69°W (not shown). One core is located near the surface (above 100 m) in the southernmost part of the section (near South America), and another, saltier, is located more to the north at deeper levels (100 to 300 m), as observed at 66°W by *Hernández-Guerra and Joyce* [2000]. Most of the flow intercepted at 35°N is within the core of the Gulf Stream, between depths 150 and 300 m, where the northeastward transport is maximum. Finally the analysis shows a main subsurface core of particles at 10°N, centered at 48°W between 70 and 170 m, and an additional smaller ensemble right at the western boundary. This distribution agrees well with the results by *Malanotte-Rizzoli et al.* [2000] showing a transfer of thermocline water from the subtropics to the tropics through both a western boundary connection and a more internal pathway. These results also remind *Worthington*'s [1976] observations of a westward salinity tongue propagating southward and toward the Caribbean Sea, and of a salty core in the center of the Gulf Stream. It is worth noting that no direct northward export from the formation area toward higher latitudes is found in the ocean interior. Near the surface, we mentioned above the role of a barrier played by the line of Ekman transport convergence near 30°N. At depth, the just-formed northern SMW is first entrained southwestward by the NEC.

4.2. Southern SMW

[20] Unlike the NH, the three possible destinations we defined for interception play an approximately equivalent role (Figure 6). The discrimination between northward and eastward-transmitted particles depends only slightly on the latitude chosen for the northernmost section, as long as the North Equatorial Countercurrent (NECC) is correctly isolated. For sake of simplicity, we kept the same section as the one used for the northern SMW. It provides a convenient discrimination between the system of equatorial currents, including the EUC, NECC and North Equatorial Undercurrent, and the subtropical dynamics. The export of salty waters from their formation region is first confined to the western boundary currents: the BC for the southward export, and the North Brazil Undercurrent (NBUC) extending into the North Brazil current (NBC) for the northward export. At 30°S (Figure 6a), all particles (2.9 Sv) are concentrated within 4° of longitude from the Brazilian coast, and their vertical distribution (not shown) revealed them to cross this latitude in the upper 200 m. At 10°N (Figures 6b and 6c, 2.7 Sv), we find two cores of particles. The first one (Figure 6b) is attached to the western boundary in the upper 150 m, that is, in the surface mixed layer. The second one is of wider zonal extension (Figure 6c, 20°W–45°W) and has a mid-depth of about 30 m. They both correspond to water that left the western boundary at the retroflection of the NBC, and was upwelled in the equatorial band to the west of 15°W, before being advected poleward by the Ekman drift of the trade winds. All the flow intercepted at 10°N participates in the transfer of warm water from the SH to the NH and the northward export diagnosed at 10°N reminds of the results shown by *Blanke et al.* [1999] in their diagnostic of the warm water paths in the equatorial Atlantic (their Figures 5, 6a, and 7a). Finally, the fraction of the flow that is intercepted at 15°W (Figure 6d, 3.0 Sv) consists mostly in EUC particles (85%), but also of particles advected by the NECC toward the Guinea Current (close to the surface and between 3°N and 8°N). The tracing of southern SMW in the EUC is in agreement with the origins of this current as diagnosed by *Metcalf and Stalcup* [1967].

4.3. Salinity Tracing Along Main Pathways

[21] The pathways diagnosed from the Lagrangian analysis account for all the observed high salinity anomalies revealing SMW that we quoted in the introduction. However, salinity is not conserved along these pathways: lateral and vertical mixing with neighboring water masses in the interior ocean, and, above all, air-sea interactions (when trajectories intercept the surface mixed layer) explain the Lagrangian salinity variations. Figure 7 sums up these conversions by showing the mean salinities and associated standard deviations at the initial (the SMW formation regions) and final (the interception sections) ends of each transfer. In the NH, the particles connecting the subtropical gyre with the Caribbean Sea are the saltiest ones, with an initial mean salinity of 37.05 psu. Both other transfers use fresher particles, with a mean salinity of 36.79 psu (respectively 36.74 psu) for 10°N (35°N). This distribution is consistent with the initial geographical positioning of the particles (see Figure 5): the center of the gyre preferentially feeds the Caribbean Sea, whereas more peripheral (hence fresher) areas feed the northward and southward exports. Such a distinction is more difficult in the SH as all particles take somewhat equivalent routes along the western boundary (see Figure 6). Nevertheless, saltiest initial waters (36.88 psu) correspond to the direct export to 10°N. The northern SMW shows a limited salinity scatter (<0.2 psu) when arriving at the interception sections. This holds true for the southern SMW arriving at 30°S. On the other hand, larger salinity dispersions are observed in the south-

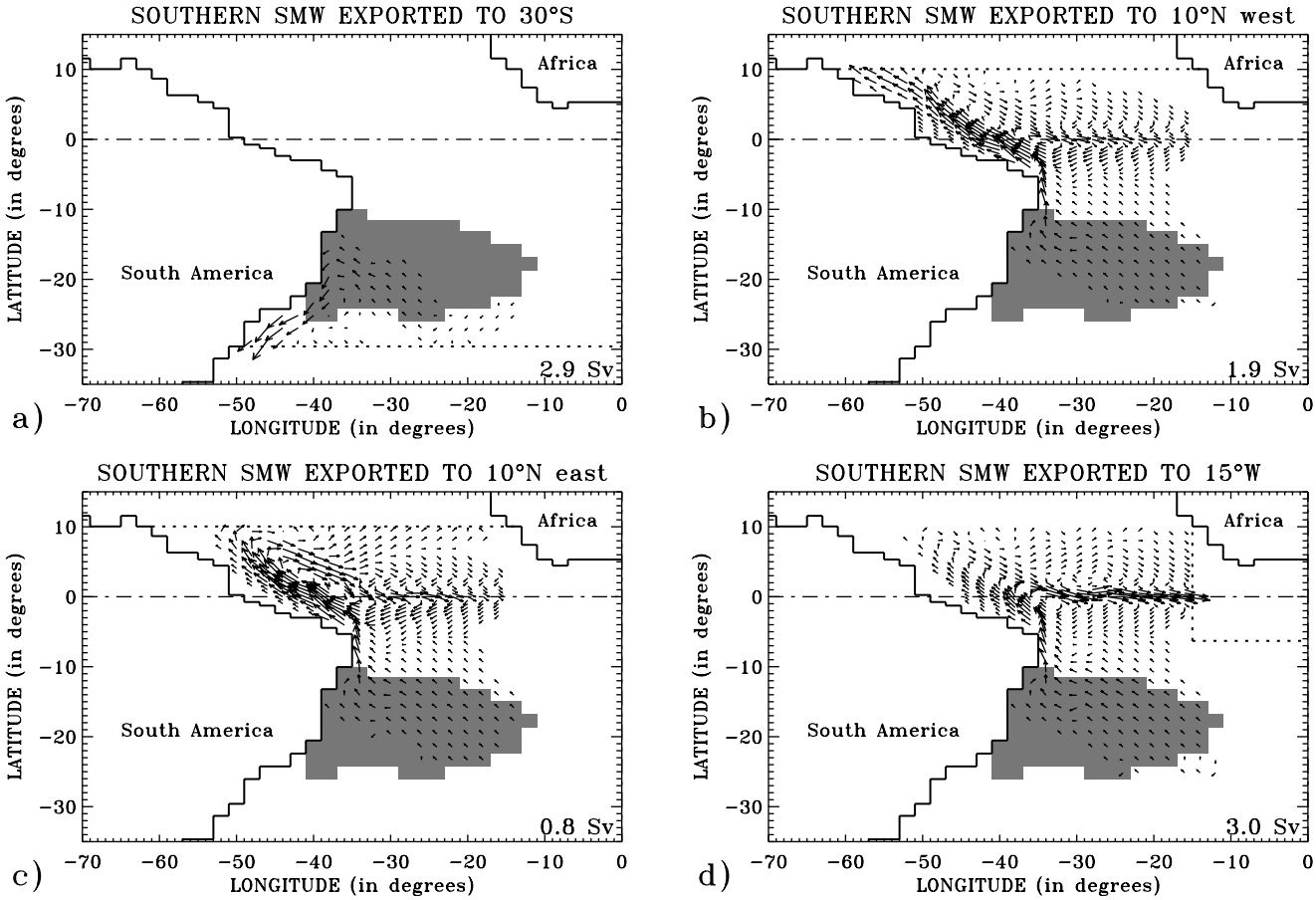

Figure 6. Same as Figure 5 but for southern SMW. (a) Transmission to 30°S. (b) Direct transmission to 10°N, west of 53°W. (c) Direct transmission to 10°N, east of 53°W. (d) Transmission to the eastern Atlantic (15°W). The region of formation of southern SMW is shaded on each panel.

ern waters arriving at 15°W and at 10°N (especially along the western boundary). The freshest mean salinity values for salinity are obtained at 10°N because a significant fraction of this water recirculates in the equatorial gyre (without reaching 15°W) and is freshened through upwelling before escaping north. On the contrary, the limit at 15°W is likely to intercept EUC particles during their first equatorial recirculation and is thus associated with saltier waters.

4.4. Seasonal Variability of SMW Formation

[22] The SMW export exhibits a strong seasonality. Figure 8 displays the monthly rate of formation calculated by summing the infinitesimal transports of the particles that are initialized on the same month and that explain true SMW export. The monthly mixed layer depth (calculated at the center of each salinity patch) is also given. SMW formation happens mostly in March (respectively September) in the NH (SH), with up to 60% (respectively 52%) of the total export being achieved during that month. It is only active over a 5-month period covering winter and spring seasons. No SMW is exported during summer or fall, whatever the hemisphere. This result agrees well with the formation mechanism of this water mass. It is first homogenized throughout the mixed layer under the influence of surface forcing (maximum evaporation and strong wind stress lead to strong vertical stirring in the mixed layer). It is then injected into the interior ocean when the mixed layer retracts abruptly under the effect of early spring surface stratification. The variability shown by the model is also in accordance with Stommel's mixed layer demon [*Stommel* 1979; *Williams et al.*, 1995] that explains the main reasons of a preferred winter water mass export for subduction. Most of the mixed layer water included in the surface layer may be detrained in the seasonal pycnocline whenever the mixed layer shallows, but the water that will further participate in genuine subduction is mostly confined to the deepest levels of the mixed layer and corresponds to an intermittent winter injection in the permanent pycnocline.

5. Extended Lagrangian Diagnostics

5.1. Poleward Export

[23] In order to investigate more thoroughly the fate of SMW we extend the first set of trajectories to new interception sections (see Figure 4). Figure 9a focuses on the particles that first entered the Caribbean Sea. It presents extended trajectory calculations till these particles eventually reach 47°N, the Gulf of Cadiz (6°W) or the southern edge of the subtropical gyre (at 22°N). Their pathways cross the Gulf of Mexico before they pass by the Straits of Florida, in agreement with observations by *Schmitz and*

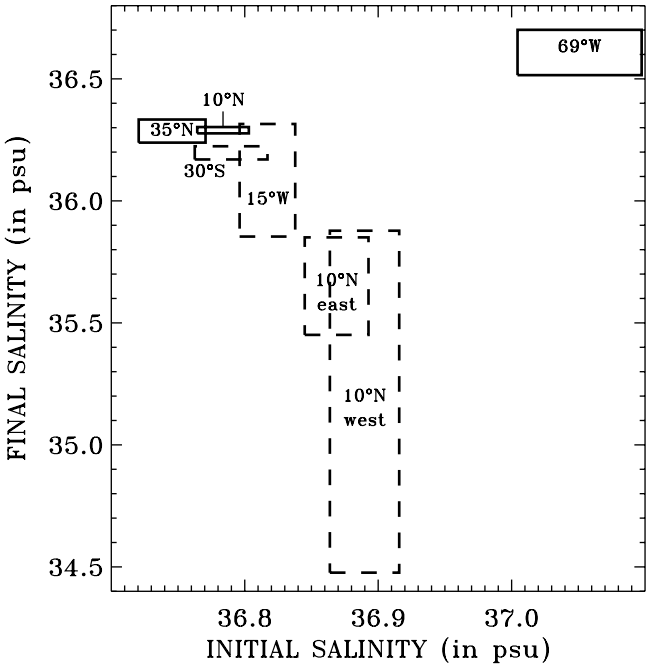

Figure 7. Salinity variations along the SMW transfers discussed in the text. Mean salinity (center of a box) and associated standard deviation (half-width of a box) are calculated from the particles (weighted by their individual transport) that describe each connection. Solid (respectively dashed) contours refer to northern (respectively southern) SMW.

Richardson [1991]. A vertical distribution of these particles at 35°N (not shown) showed them to be grouped close to the western edge of the Gulf Stream, within the upper 400 m of the ocean. Despite their long journey from the SMW formation region, they still explain a high salinity subregion of the Gulf Stream, probably because they were among the saltiest initial particles (see Figure 7). Half of the SMW transiting through the Caribbean Sea is transmitted to 47°N

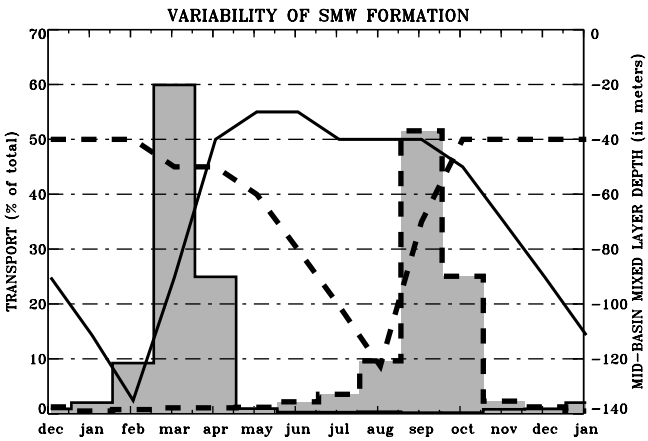

Figure 8. Seasonal variability for SMW formation as a monthly histogram (left-hand axis), and midbasin mixed layer depth (right-hand axis). Solid (respectively dashed) lines refer to the NH (SH). SMW monthly exports are given as percentages of the total annual values.

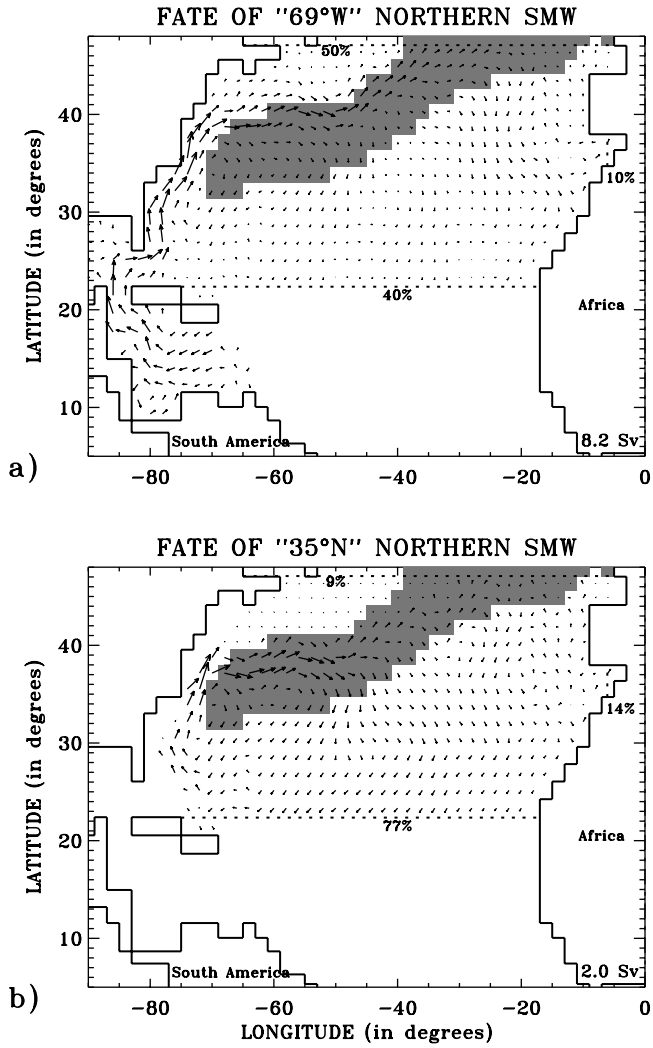

Figure 9. Same as Figure 5 but for new interception sections set at 47°N and 22°N. (a) For the particles exported initially to the Caribbean Sea (69°W). (b) For the particles exported initially to 35°N. The region of maximum winter mixed layer depth higher than 180 m (Figure 1b) is shaded and shows the domain of formation of the 18°C-water (to the west of ~40°W).

within the North Atlantic Current, 40% loops back to the subtropics following preferably a southward return route in the eastern Atlantic [see *Blanke et al.*, 2002b], and 10% enters the Gulf of Cadiz. Extending the set of particles first intercepted at 35°N (without transit in the Caribbean Sea) to the same final sections gives a different result (Figure 9b), with more than 75% of the transport recirculating southward, the rest of which being transmitted either northward or eastward to 6°W. The SMW transmitted to 35°N north of the West Indies is originally less salty than the component that crosses the Caribbean Sea. This distinction still holds at 35°N: at this latitude, these less saline waters being observed at a shallower depth are more sensitive to the direct action of the surface wind stress, and thus recirculate southward more easily.

[24] Extended trajectories have also been calculated for the SH, using new interception sections at 21°S, 45°S and

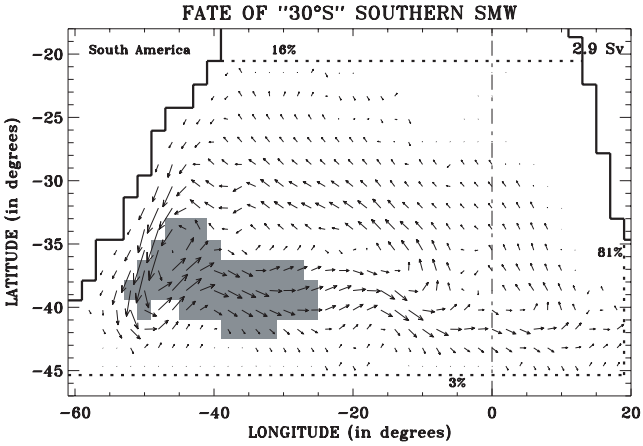

Figure 10. Same as Figure 5 but for the waters already exported initially to 30°S from the southern SMW formation region, and for new interception sections set at 19°E, 21°S and 45°S. The region of maximum winter mixed layer deeper than 180 m (Figure 1b) is shaded and shows the domain of formation of STMW.

19°E for the particles initially stopped at 30°S (Figure 10). Some intense recirculation is observed in the subtropical gyre between 30°S and 40°S. Then, most of the flow (2.1 Sv) is carried eastward by the South Atlantic Current, before an eventual transmission to the Indian Ocean. This vein of current is concentrated in a narrow 41–44°S latitude band, immediately south of the Agulhas Current. The interception section at 21°S (0.4 Sv) shows an ensemble of particles at depths close to 500 m being conveyed northward by the NBUC after recirculation in the subtropical gyre. As observed by *Stramma and England* [1999], the separation between the NBUC and the surface-intensified BC shifts southward with increasing depth, and the section at 21°S intercepts the NBUC at the level of subthermocline waters.

[25] Coming back to Figure 1b, strong maxima of the mixed layer depth are observed poleward of the weaker SMW maxima in both hemispheres, at latitudes higher than 30 degrees. These are the regions of formation of the STMWs: in the North Atlantic, the western half of this region is where the so-called 18°C-water is formed [*Worthington*, 1959]. Colder varieties of STMW are formed farther northeast [*McCartney and Talley*, 1982]. Although in the South Atlantic the domain of deep mixed layer is confined to the western basin, winter convection is also known to create a variety of thermostads between 12°C and 17°C in this region [*Gordon*, 1981; *McCartney*, 1982]. *Gordon* [1981] pointed out that the supply of saline near-surface water (namely SMW) to this region by the BC is a destabilizing factor favoring the vertical homogenization, and results in high salinity anomalies in the Central Water (CW) θ-S diagram. Having superimposed the STMW formation regions onto the SMW circulation maps of Figures 9 and 10, we indeed observe a supply of SMW to the southern STMW domain (Figure 10). The figure even exhibits some recirculation of the SMW in the Brazil Return Current, which, through a lasting contact with the atmosphere, is a likely favorable condition for water mass conversion. Following the property modifications of the particles involved in this path (not shown) indeed indicated a cooling and freshening (to ∼13°C and 35.2 psu) of the SMW in this region. To our knowledge, no equivalent contribution of the northern SMW to the 18°C-water has been reported and, unlike the STMW of the western Argentine Basin, the northern STMW does not show any pronounced θ-S anomaly relative to the surrounding North Atlantic CW. On Figure 9 we do observe, however, that the SMW feeds the region of formation of the 18°C-water, and an 18°C plateau was noticed on the temperature tracing of selected particles. These are signs of a mechanism comparable to the one operating in the South Atlantic.

5.2. Equatorward Export

[26] The equatorward transmission of SMW takes place in the framework of the STCs that connect the subtropics to the equatorial domain. The equatorward limbs of these cells have been mostly investigated by means of numerical models, either in simple geometrical configurations [*Liu*, 1993; *Liu et al.*, 1994], or more recently by *Malanotte-Rizzoli et al.* [2000] and *Lazar et al.* [2001] for a more accurate Atlantic geometry. In all cases, two dominant equatorward paths appear, either through the western boundary current system, or within the interior ocean. The specificity of the North Atlantic compared to the southern basin lies in the presence of the ITCZ (and the induced NECC) that may prevent the subducted flow to reach the equator. The southern connection is more obvious, as shown by *Schott and Böning* [1991] from model results, with the SEC feeding the NBUC and then the EUC. These model results were confirmed by *Stramma et al.* [1995] documenting the vertical structure of the NBUC.

[27] The overturning stream function is calculated from the time and zonal integration of the model meridional and vertical velocity components (Figure 11). It provides a fast diagnostic of these cells, though it offers only a 2D vision, dropping some of the complexity of the 3D circulation. The equatorial upwelling between 2°S and 2°N amounts to 13 Sv, and balances an equivalent surface poleward flux. The maximum of the stream function at 2°S and depth 50 m defines an approximate core of the southern STC, with roughly 8 Sv. The eastward flowing NECC and NEUC in

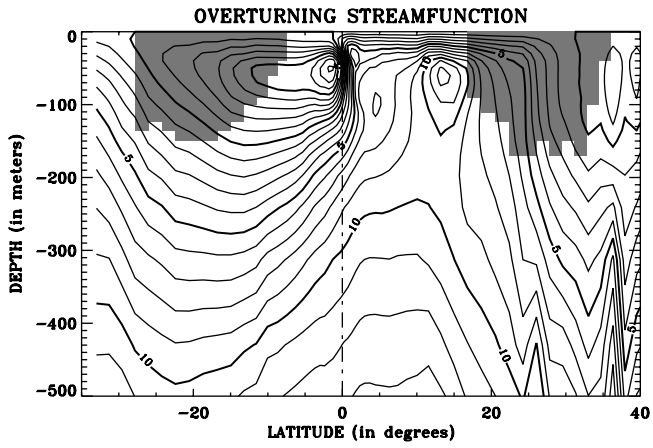

Figure 11. Annual mean zonally integrated circulation. The contour interval is 1 Sv. The shading represents the initial locations of the SMW particles.

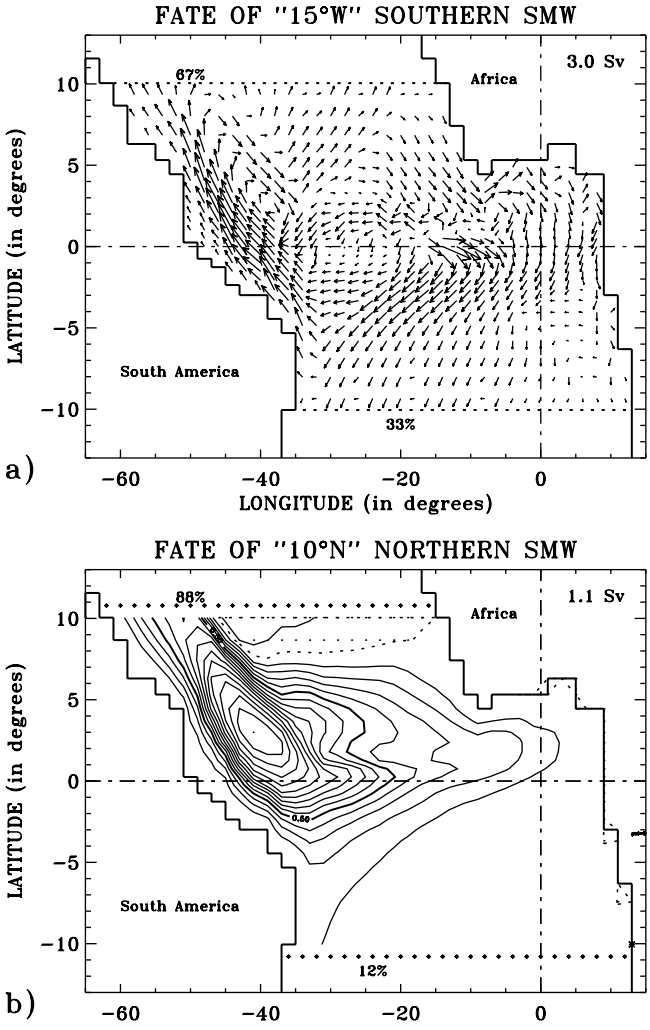

Figure 12. (a) Same as Figure 5 but for the particles exported initially to 15°W from the southern SMW formation region, and for new interception sections set at 10°N and 10°S. (b) Horizontal mass stream function related to the equatorial recirculation of northern SMW originating in 10°N (see *Blanke et al.* [1999] for details about the calculation). The value of the stream function is set arbitrarily to 0 above Africa. Negative values are dotted. The contour interval is 0.1 Sv.

the NH and the net northward transfer of warm waters make its northern counterpart less obvious. A first maximum (12 Sv) is visible at 13°N and depth 60 m, but a secondary core appears closer to the equator (2°N, 30 m). In Figure 11, the two shaded domains, showing the zonal projection of the SMW particles initial positions, represent the formation areas in this depth-latitude display. Although some aspects of the SMW circulation are masked in the basin-wide zonal integration, others are suggested. In the SH, one is the part played by the equatorward limb of the STC in the subduction of the SMW. There is no indication, however, of the poleward export of southern SMW, probably because this export by the BC is compensated in the zonal integration by the equatorward component of the SEC in the ocean interior. Figure 11 suggests entrainment of the subducted southern SMW in the equatorial upwelling, and subsequent sharing of it by the opposite Ekman drifts of the two hemispheres. While a fraction of the water caught by the upper limb of the southern STC may reenter the southern formation region, there is indication in Figure 11 that the northbound part may contribute to the supply of the northern SMW formation area. The eventual northward direction taken by most of the subducted northern SMW is reproduced in Figure 11, although the details are not. For instance, the southward component of the subducting water en route for the 69°W line is not seen, as it is compensated in the basin-wide average by the northward flow of the Caribbean Sea. There is also no sign of any subducted northern SMW being trapped in the equatorward limb of the STC, probably for the same reason combined with the weak transport along this route.

[28] To further investigate the interplay of SMW and STCs, we extended the trajectories of the particles initially stopped at 10°N or 15°W toward new limits set at 10°S and again at 10°N, close to the centers of both STCs (Figure12). Southern SMW is seen to feed the EUC in agreement with known features of EUC origins [*Taft*, 1963]. Particles captured by the EUC are slowly upwelled along the equator before turning southwestward in the eastern Atlantic where they join the central branch of the SEC. They finally reach the NBUC at the west coast and escape northward (Figure 12a, 2.0 Sv). A fraction of the flow recirculates several times within the equatorial gyre. As already shown by *Blanke et al.* [1999], the interception section at 10°S intercepts a fraction of the southward Ekman drift (here 1.0 Sv). The equatorial circulation of northern SMW may be given as a horizontal mass stream function [see *Blanke et al.*, 1999] since no particle is initialized or stopped inside the domain in study (Figure 12b). Almost all the flow recirculates to 10°N (1.0 out of 1.1 Sv). It feeds the NECC, proceeds equatorward and upwells, then crosses the Atlantic southwestward in the central branch of the SEC. This recirculation in the equatorial gyre (within the NECC, EUC, and SEC) is visible before the export to 10°N along the coast of South America.

6. Feeding of the Formation Areas

6.1. SMW Backward Tracing

[29] We integrate backward in time the trajectories of the particles that explained a true export of SMW from the formation regions, accounting for 11.3 Sv (respectively 8.6 Sv) in the NH (SH), till they reach one of the interception sections we already defined in section 3. The set of initial positions for this new tracing is thus exactly the same as before, right over the envelope of the mixed layer, but now we transport the particles with the OGCM monthly velocity multiplied by −1 and ordered backward in time. Figure 13 shows the results in terms of a vector transport field (as in Figure 5). In the NH, the supply of water is distributed almost equally between 35°N (6.0 Sv) and 10°N (4.9 Sv), with an additional contribution from the Straits of Florida (0.4 Sv). The water coming from 10°N is conveyed to the northern formation region mostly in a near-surface layer by the Ekman drift of the trade winds, as hinted from Figure 11. In the SH, SMW draws its waters from the equator (4.0 Sv at 6°S and 2.6 Sv at 15°W), also within the near-surface layer,

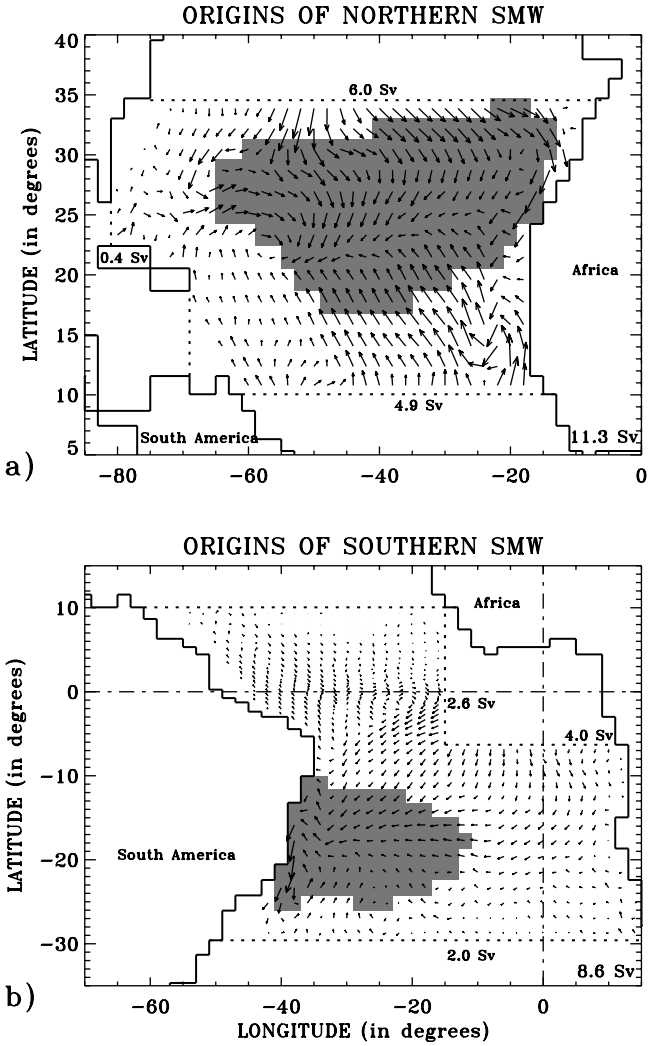

Figure 13. Vertically integrated transport of the flow feeding both SMW formation regions, for backward interception sections identical to those used in subsection 3.3. Arrows' size is normalized by the length of the largest transport of each panel, and smaller transports are enlarged for better readability. (a) Northern Hemisphere. (b) Southern Hemisphere. The SMW formation regions are shaded.

and from the South Atlantic (2.0 Sv) within the southern branch of the SEC.

6.2. Subtropical Salinity Increase

[30] Akin to oceanic concentration basins, the SMW formation areas as defined in this study may be regarded as ''concentration regions'' of variable geometry in the ocean interior, characterized by inflowing waters that have a weaker salinity and excess volume transport relative to the outflowing waters, on account of the net fresh water loss through evaporation. Because of the mass-preserving character of the model, the slight difference between the incoming and outflowing volume transports is not reproduced, yet an approximate diagnostic of the fresh water loss at the surface of the formation areas can be obtained using the export volume transports. The salt inflow, $[\boldsymbol{S}]^{\text{inflow}}$, and outflow, $[\boldsymbol{S}]^{\text{outflow}}$, in the model, may be calculated by multiplying each infinitesimal transport by the surrounding salinity at the entry and exit points of the SMW formation domains in both hemispheres, and by summing the product over the whole set of particles:

$$[\mathbf{S}]^{\text{inflow}} = \sum_{p=1}^{N} Tr_p \, \rho_p^{\text{inflow}} S_p^{\text{inflow}} \tag{2}$$

$$[\mathbf{S}]^{\text{outflow}} = \sum_{p=1}^{N} Tr_p \, \rho_p^{\text{outflow}} S_p^{\text{outflow}} \tag{3}$$

where N is the total number of particles and Tr denotes each individual transport with

$$\sum_{p=1}^{N} Tr_p^{\text{NH}} = 11.3 \; Sv \tag{4}$$

$$\sum_{p=1}^{N} Tr_p^{\text{SH}} = 8.6 \; Sv \tag{5}$$

and where ρ and S refer to the density and salinity at each particle's location. The resulting salt fluxes are expressed in grams per second, assimilating psu units to grams per kilogram. Table 3 reports the values obtained for both hemispheres. One can convert the difference between $[\boldsymbol{S}]^{\text{outflow}}$ and $[\boldsymbol{S}]^{\text{inflow}}$ to a net fresh water flux to the atmosphere, after normalization by a mean salinity and a mean density. We obtain 0.125 Sv (respectively 0.077 Sv) in the NH (SH). From the annual mean area of each salinity patch, we derive mean evaporation minus precipitation rates equal to 60 cm/yr (respectively 55 cm/yr). The value obtained for the NH is in agreement with the annual map proposed by *Schmitt et al.* [1989], which displays rates ranging from 50 to 150 cm/yr.

7. Discussion and Summary

[31] We have investigated the export and fate of the SMW formed in the subtropics of the Atlantic Ocean by means of a Lagrangian tracing in an OGCM. Appropriate definitions of the formation regions based on the SMW formation mechanisms allowed us to estimate rates of export of 11.3 Sv (respectively 8.6 Sv) in the NH (SH). These values were shown to depend on the lateral limit of the formation areas, chosen at the surface isohaline 36.6. Whereas this choice rested on objective grounds in the North Atlantic, a possible lower value of 36.4 in the South Atlantic would have led to a formation rate 11.2 Sv, comparable to that of the northern

Table 3. Subtropical Salt Fluxes[a]

Hemisphere	Entering the Patch	Subducting	Difference
Northern	4.22×10^{11}	4.27×10^{11}	4.6×10^{9}
Southern	3.19×10^{11}	3.22×10^{11}	2.8×10^{9}

[a] Values are in g/s, diagnosed in the model at the entry (first column) and exit (second column) of the SMW formation area, and their differences (third column) used for estimations of the fresh water loss to the atmosphere.

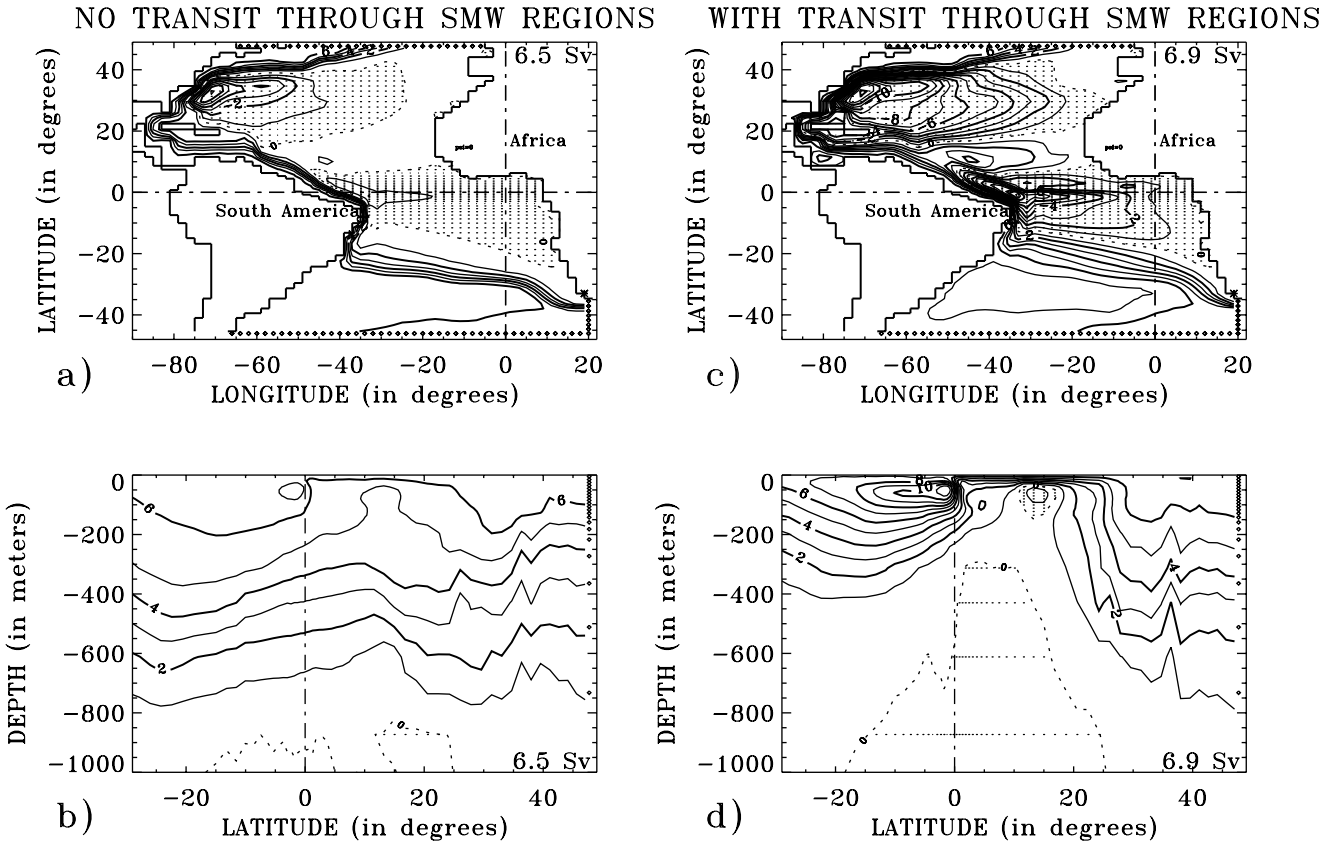

Figure 14. Mass stream function related to the southern origins (45°S or 19°E) of the northward flow considered at 47°N (see *Blanke et al.* [1999] for details about the calculation). Negative values are dotted. The contour interval is 1 Sv. Calculations are done separately for the particles that avoid (panels a and b) or transit through (panels c and d) the SMW formation regions. (a) and (c) Horizontal projection, with the value of the stream function set arbitrarily to 0 above Africa. (b) and (d) Vertical projection, with the value of the stream function set arbitrarily to 0 at the ocean bottom.

SMW. Despite this degree of arbitrariness on the southern export rate and transports along the subsequent routes, the analysis of the pathways and remote fates of the SMW were found to match the scattered available observations. They also revealed pronounced asymmetries in the behaviors of the southern and northern varieties of SMW: while the export of the former is realized almost exclusively by the western boundary currents, that of the latter mostly results from interior subduction. Also, in agreement with the net northward transport of upper waters in the Atlantic, most of the southern SMW flows equatorward (5.7 Sv out of 8.6 Sv), and its northern counterpart largely turns poleward (10.2 Sv out of 11.3 Sv).

[32] In this final discussion, we mention briefly the role of the SMW in the context of the whole Atlantic Ocean in relation to the northward salinity increase of the Atlantic upper waters. Our analysis in terms of close and remote destinations of the SMW does not allow us to determine the contribution of the SMW to the flow that eventually reach the high latitudes of the Atlantic. We found a transport of 4.6 Sv of northern SMW reaching 47°N, but this is certainly an underestimation, as a part of the water mass intersected at 22°N in Figure 9 would have probably reached 47°N if tracked during a longer time. Similarly, we found a northward SMW interhemispheric transfer of 4.7 Sv but, as a part of this water later transits through the region of formation of northern SMW, it should not be counted in addition to the latter. In order to apprehend better the role of the SMW in the context of the conveyor belt return flow, we carried out a backward integration on the particles that flow northward at 47°N in the model. In this experiment, the individual trajectories originating in the southern Atlantic were stopped at a boundary formed of segments of the 45°S parallel and 19°E meridian (Figure 14), with the particles transiting through the SMW formation regions being marked for an estimation of their transport (Table 4). This northward

Table 4. Volume Transport of the Water Flowing Northward at 47°N and Originating in the Southern Atlantic at 45°S and 19°E[a]

Behavior	Origins		Total
	19°E	45°S	
No transit through the SMW regions	5.7	0.8	6.5
Transit through the southern SMW region	1.1	0.1	1.2
Transit through the northern SMW region	2.8	0.9	3.7
Transit through both SMW regions	1.8	0.2	2.0
Total	11.4	2.0	13.4

[a] Values are in Sv. Fractions of the total transport that transits through the southern SMW and northern SMW formation regions are specified.

transfer is conveniently displayed by means of a stream function, either on a horizontal (Figures 14a and 14c) or vertical (Figures 14b and 14d) plane. It reminds us of the structure of the warm route pictured by *Speich et al.* [2001], with a dominant contribution from the Indian Ocean (11.4 Sv) and a weak direct northward transfer from the southernmost Atlantic domain (2.0 Sv). The figure differentiates the routes for the particles avoiding (Figures 14a and 14b) or being conveyed through (Figures 14c and 14d) the northern or southern SMW formation regions. This latter route (6.9 Sv) proves very sensitive to the circulation induced by the equatorial upwelling, and the horizontal equatorial, tropical and subtropical gyres. As already suggested, the total contribution of the southern SMW formation region (3.2 Sv) is smaller than the northern one (5.7 Sv). The route avoiding these SMW regions accounts for 6.5 Sv and appears more direct as it is mostly related to intermediate waters entering the Atlantic south of Africa.

[33] The above results referring to the volume transports provide no immediate information on the capacity of the SMW to increase the salinity of the Atlantic upper waters. An Eulerian integrated approach may be more appropriate, such as the one proposed by *Gordon and Piola* [1983], who presented the meridional distribution of the mean salinity for waters less dense than $\sigma_\theta = 27.6$, obtained from hydrographic transatlantic sections. This distribution (their Figure 3) shows an average northward trend of $\sim$0.5 psu from 35°S to 45°N, with two well-defined regions of higher northward increase at 30°S–20°S and 10°N–25°N, on the southern sides of both SMW formation regions, separated by a relative minimum at 5°S–5°N. The northern increase ($\sim$1 psu) is much more pronounced than the southern one ($\sim$0.3 psu), an indication of the higher contribution of the northern SMW to the upper Atlantic salinity increase. This is in keeping with the high northward transport of northern SMW and the near cancellation of the southern SMW effect by a downstream freshening in the equatorial band.

[34] The transfer of the high salinities of the northern SMW to the whole layer of CW seems to be effected by several mechanisms. One, which takes place in an area of limited extent to the northeast of the Venezuelan coast (8°N–16°N, 47°W–58°W), was analyzed by *Schmitt et al.* [1987]. In this region, the SMW flowing southeastward toward the Caribbean Sea (Figure 5a) overlies relatively fresh CW and Intermediate Water from the South Atlantic. This sets up an intense double-diffusive activity in the Central Water, recognized by a thermohaline staircase that covers most of the area. *Schmitt et al.* [1987] point out the ensuing conversion of Central Water with South Atlantic characteristics to North Atlantic Central Water. The latitudes where this conversion takes place match those of the major northward salinity increase in the meridional salinity distribution of *Gordon and Piola* [1983].

[35] The downward transfer of the SMW high salinities by double diffusion is only partial, however, as the salinity signature of the water mass is detected farther downstream in the Straits of Florida. Another process for the vertical mixing of the SMW could be winter convection leading to the formation of 18°C-water, as the northbound northern SMW was seen to feed the region where this water mass forms (Figure 9). This second process, however, has been less documented in the North Atlantic than in the southern basin [*Gordon*, 1981]. As the northern SMW is the lightest Mode Water in the North Atlantic, this mechanism, if confirmed, would amount to a first step in the Mode Water cascade toward higher densities that eventually leads to the formation of deep waters.

[36] **Acknowledgments.** We wish to thank Sabrina Speich for many useful discussions. Most of the study was initiated during the stage de Diplôme d'Enseignement Approfondi of GP at LPO. Support for this study has been provided by the Centre National de la Recherche Scientifique (CNRS) for B.B., the Institut Français de Recherche pour l'Exploitation de la Mer (IFREMER) for M.A., and the École Normale Supérieure de Lyon for G.P. Lagrangian calculations were performed with the computational resources available at LPO, at the Centre de Brest of IFREMER, and at the CNRS Institut du Développement et des Ressources en Informatique Scientifique.

References

Arakawa, A., Design of the UCLA general circulation model. Numerical simulation of weather and climate, *Tech. Rep. 7*, 116 pp., Dept. of Meteorol., Univ. of Calif., Los Angeles, 1972.

Baumgartner, A., and E. Reichel, *The World Water Balance: Mean Annual Global, Continental and Maritime Precipitation, Evaporation and Run-Off*, Elsevier Sci., New York, 1975.

Blanke, B., and S. Raynaud, Kinematics of the Pacific Equatorial Undercurrent: A Eulerian and Lagrangian approach from GCM results, *J. Phys. Oceanogr.*, *27*, 1038–1053, 1997.

Blanke, B., M. Arhan, G. Madec, and S. Roche, Warm water paths in the equatorial Atlantic as diagnosed with a general circulation model, *J. Phys. Oceanogr.*, *29*, 2753–2768, 1999.

Blanke, B., S. Speich, G. Madec, and R. Maugé, A global diagnostic of interior ocean ventilation, *Geophys. Res. Lett.*, in press, 2002a.

Blanke, B., M. Arhan, S. Speich, and K. Pailler, Diagnosing and picturing the North Atlantic segment of the global conveyor belt by means of an ocean general circulation model, *J. Phys. Oceanogr.*, *32*, 1430–1451, 2002b.

Broecker, W. S., The great ocean conveyor, *Oceanography*, *4*, 79–89, 1991.

Döös, K., Interocean exchange of water masses, *J. Geophys. Res.*, *100*, 13,499–13,514, 1995.

Gordon, A. L., South Atlantic thermocline ventilation, *Deep Sea Res.*, *28*, 1239–1264, 1981.

Gordon, A. L., Comment on the South Atlantic's role in the global circulation, in *The South Atlantic: Present and Past Circulation*, edited by G. Wefer et al., pp. 121–124, Springer-Verlag, New York, 1996.

Gordon, A. L., and A. P. Piola, Atlantic Ocean upper layer salinity budget, *J. Phys. Oceanogr.*, *13*, 1293–1300, 1983.

Gordon, A. L., R. F. Weiss, W. M. Smethie Jr., and M. J. Warner, Thermocline and intermediate water communication between the South Atlantic and Indian Oceans, *J. Geophys. Res.*, *97*, 7223–7240, 1992.

Hernández-Guerra, A., and T. M. Joyce, Water masses and circulation in the surface layers of the Caribbean at 66°W, *Geophys. Res. Lett.*, *27*, 3497–3500, 2000.

Jenkins, W. J., ^{3}H and ^{3}He in the Beta triangle: Observations of gyre ventilation and oxygen utilization rates, *J. Phys. Oceanogr.*, *17*, 763–783, 1987.

Jenkins, W. J., The use of anthropogenic tritium and helium-3 to study subtropical gyre ventilation and circulation, *Philos. Trans. R. Soc. London, Ser. A*, *325*, 43–61, 1988.

Lazar, A., R. Murtugudde, and A. J. Busalacchi, A model study of temperature anomaly propagation from the subtropics to tropics within the South Atlantic thermocline, *Geophys. Res. Lett.*, *28*, 1271–1274, 2001.

Lazar, A., T. Inui, A. J. Busalacchi, P. Malanotte-Rizzoli, L. Wang, and R. Murtugudde, Seasonality of the ventilation of the tropical Atlantic thermocline in an OGCM, *J. Geophys. Res.*, in press, 2002.

Levitus, S., *Climatological Atlas of the World Ocean*, *NOAA Prof. Pap. 13*, 173 pp., U.S. Govt. Print. Off., Washington, D.C., 1982.

Liu, Z., A simple model of the mass exchange between the tropical and subtropical ocean, *J. Phys. Oceanogr.*, *24*, 1153–1165, 1993.

Liu, Z., S. G. H. Philander, and R. C. Pacanoswki, A GCM study of tropical-subtropical upper-ocean water exchange, *J. Phys. Oceanogr.*, *24*, 2606–2623, 1994.

Madec, G., and M. Imbard, A global ocean mesh to overcome the North Pole singularity, *Clim. Dyn.*, *12*, 381–388, 1996.

Madec, G., P. Delecluse, M. Imbard, and C. Lévy, OPA 8.1 Ocean General Circulation Model reference manual, *Notes du Pôle de Modélisation de l'Institut Pierre-Simon Laplace*, 11, 91 pp., available from LODYC,

Univ. Pierre et Marie Curie–Case 100, 4 place Jussieu, 75252 Paris Cedex 05, France, 1998.
Malanotte-Rizzoli, P., K. Hedstrom, H. Arango, and D. B. Haidvogel, Water mass pathways between the subtropical and tropical ocean in a climatological simulation of the North Atlantic ocean circulation, *Dyn. Atmos. Oceans*, *32*, 331–371, 2000.
Marshall, J. C., A. J. G. Nurser, and R. G. Williams, Inferring the subduction rate and period over the North Atlantic, *J. Phys. Oceanogr.*, *23*, 1315–1329, 1993.
Marshall, J. C., D. Jamous, and J. Nilsson, Reconciling thermodynamic methods of computation of water-mass transformation rates, *Deep Sea Res.*, *Part I*, *46*, 545–572, 1999.
McCartney, M. S., The subtropical recirculation of Mode Waters, *J. Mar. Res.*, *40*(suppl.), 427–464, 1982.
McCartney, M. S., Crossing of the equator by the Deep Western Boundary Current in the Atlantic Ocean, *J. Phys. Oceanogr.*, *23*, 1953–1974, 1993.
McCartney, M. S., and L. D. Talley, The subpolar Mode Water of the North Atlantic Ocean, *J. Phys. Oceanogr.*, *12*, 1169–1188, 1982.
Mémery, L., M. Arhan, A. Alvarez-Salgado, M.-J. Messias, H. Mercier, C. G. Castro, and A. F. Rios, The water masses along the western boundary of the south and equatorial Atlantic, *Prog. Oceanogr.*, *47*, 69–98, 2000.
Metcalf, W. G., and M. C. Stalcup, Origin of the Atlantic Equatorial Undercurrent, *J. Geophys. Res.*, *72*, 4959–4975, 1967.
Nurser, A. J. G., and J. C. Marshall, On the relationship between subduction rates and diabatic forcing of the mixed layer, *J. Phys. Oceanogr.*, *21*, 1793–1802, 1991.
O'Connor, B., R. A. Fine, K. A. Maillet, and D. B. Olson, The rate of formation of the Subtropical Underwater (STUW) in the North and South Pacific from drifter and tracer data, *Int. WOCE Newsl.*, *31*, 18–20, 1998.
Qiu, B., and R. X. Huang, Ventilation of the North Atlantic and North Pacific: Subduction versus obduction, *J. Phys. Oceanogr.*, *25*, 2374–2390, 1995.
Reid, J. L., On the temperature, salinity, and density differences between the Atlantic and Pacific oceans in the upper kilometer, *Deep Sea Res.*, *7*, 265–275, 1961.
Schmitt, R. W., H. Perkins, J. D. Boyd, and M. C. Stalcup, C-Salt: An investigation of the thermohaline staircase in the western tropical North Atlantic, *Deep Sea Res.*, *34*, 1655–1665, 1987.
Schmitt, R. W., P. S. Bogden, and C. E. Dorman, Evaporation minus precipitation and density fluxes for the North Atlantic, *J. Phys. Oceanogr.*, *19*, 1208–1221, 1989.
Schmitz, W. J., and P. L. Richardson, On the sources of the Florida Current, *Deep Sea Res.*, *38*(suppl. 1), S379–S409, 1991.
Schott, F. A., and C. W. Böning, Evaluation of the WOCE model in the western equatorial Atlantic: Upper layer circulation, *J. Geophys. Res.*, *96*, 6993–7004, 1991.
Smith, W. H. F., and D. T. Sandwell, Global sea floor topography from satellite altimetry and ship depth soundings, *Science*, *277*, 1956–1962, 1997.
Speer, K. G., and E. Tziperman, Rates of water mass formation in the North Atlantic ocean, *J. Phys. Oceanogr.*, *22*, 93–104, 1992.
Speer, K. G., H.-J. Isemer, and A. Biastoch, Water mass formation from revised COADS data, *J. Phys. Oceanogr.*, *25*, 2444–2457, 1995.
Speich, S., B. Blanke, and G. Madec, Warm and cold water paths of a GCM thermohaline conveyor belt, *Geophys. Res. Lett.*, *28*, 311–314, 2001.
Sprintall, J., and M. Tomczak, Evidence of the Barrier Layer in the surface layer of the tropics, *J. Geophys. Res.*, *97*, 7305–7316, 1992.
Stommel, H., Determination of water mass properties of water pumped down from the Ekman layer to the geostrophic flow below, *Proc. Natl. Acad. Sci. U. S. A.*, *76*, 3051–3055, 1979.
Stramma, L., and M. England, On the water masses and mean circulation of the South Atlantic Ocean, *J. Geophys. Res.*, *104*, 20,863–20,883, 1999.
Stramma, L., and F. Schott, Western Equatorial circulation and interhemispheric exchange, in *The Warmwatersphere of the North Atlantic Ocean*, edited by W. Krauss, pp. 195–227, Gebrüder Borntraeger, Berlin, 1996.
Stramma, L., J. Fisher, and J. Reppin, The North Brazil Undercurrent, *Deep Sea Res.*, *42*, 773–795, 1995.
Taft, B. A., Distribution of salinity and dissolved oxygen on surfaces of uniform potential specific volume in the South Atlantic, South Pacific, and Indian Oceans, *J. Mar. Res.*, *21*, 129–146, 1963.
Tsuchiya, M., L. D. Talley, and M. S. McCartney, An eastern Atlantic section from Iceland southward across the equator, *Deep Sea Res.*, *39*, 1882–1917, 1992.
Tsuchiya, M., L. D. Talley, and M. S. McCartney, Water-mass distributions in the western South Atlantic: A section from South Georgia Island (54°S) northward across the equator, *J. Mar. Res.*, *52*, 55–81, 1994.
Wacongne, S., and B. Piton, The near-surface circulation in the northeastern corner of the south Atlantic ocean, *Deep Sea Res.*, *7/8*, 1273–1298, 1991.
Walin, G., On the relation between sea-surface heat flow and thermal circulation in the ocean, *Tellus*, *34*, 187–195, 1982.
Wienders, N., M. Arhan, and H. Mercier, Circulation at the western boundary of the South and equatorial Atlantic: Exchanges with the interior ocean, *J. Mar. Res.*, *58*, 1007–1039, 2000.
Williams, R. G., M. A. Spall, and J. C. Marshall, Does Stommel's mixed-layer "demon" work?, *J. Phys. Oceanogr.*, *25*, 3089–3102, 1995.
Woods, J. D., The physics of the thermocline ventilation, in *Coupled Ocean-Atmosphere Models*, pp. 543–590, Elsevier Sci., New York, 1985.
Worthington, L. V., The 18° Water in the Sargasso Sea, *Deep Sea Res.*, *5*, 297–305, 1959.
Worthington, L. V., On the North Atlantic Circulation, *Johns Hopkins Oceanogr. Stud., 6*, 110 pp., Johns Hopkins Univ. Press, Baltimore, Md., 1976.

M. Arhan, Laboratoire de Physique des Océans, Ifremer Brest, BP 70, 29280 Plouzané, France. (marhan@ifremer.fr)

B. Blanke and G. Prévost, Laboratoire de Physique des Océans, UFR Sciences et Techniques, 6 avenue Le Gorgeu, BP 809, 29285 Brest, France. (blanke@univ-brest.fr)

A. Lazar, Laboratoire d'Océanographie Dynamique et de Climatologie, Université Pierre et Marie Curie, Case 100, 4 place Jussieu, 75256 Paris, Cedex 05, France. (ala@lodyc.jussieu.fr)